

# Synthesis of Low-Melting Metal Oxide and Sulfide Nanowires and Nanobelts

R. RAO,<sup>1</sup> H. CHANDRASEKARAN,<sup>2</sup> S. GUBBALA,<sup>2</sup> M.K. SUNKARA,<sup>2</sup>  
C. DARAIO,<sup>3</sup> S. JIN,<sup>3</sup> and A.M. RAO<sup>1,4</sup>

1.—Department of Physics and Astronomy, Clemson University, Clemson, SC, 29634.

2.—Department of Chemical Engineering, University of Louisville, Louisville, KY, 40292.

3.—Department of Materials Science, University of California—San Diego, La Jolla, CA, 92093.

4.—E-mail: arao@clemson.edu

The bulk nucleation and basal growth of semiconducting nanowires from molten Ga pools has been demonstrated earlier using oxygen/hydrogen plasma over molten Ga pools. Herein, we extend the above concept for bulk synthesis of oxide and sulfide nanowires of low-melting metal melts such as Sn and In. Specifically, nanowires of  $\beta$ -Ga<sub>2</sub>O<sub>3</sub>,  $\beta$ -In<sub>2</sub>O<sub>3</sub>, SnO<sub>2</sub>,  $\alpha$ -Ga<sub>2</sub>S<sub>3</sub>, and  $\beta$ -In<sub>2</sub>S<sub>3</sub> were synthesized using direct reactions between respective molten metal pools and the gases such as oxygen/hydrogen mixture for oxides and H<sub>2</sub>S for sulfides. In the case of  $\beta$ -Ga<sub>2</sub>O<sub>3</sub> and SnO<sub>2</sub>, a change in the morphology from nanowires to nanobelts was observed with an increase in the synthesis temperature. No such behavior was observed in the case of  $\beta$ -In<sub>2</sub>O<sub>3</sub>. Furthermore, we present evidence for  $\alpha$ -Ga<sub>2</sub>S<sub>3</sub> nanowires, which to our knowledge is being reported for the first time in the literature. Our studies with the sulfide nanowires suggest that H<sub>2</sub>S reacts directly at the molten metal surface to form gallium sulfide. Finally, we discuss the role of chamber pressure and hydrogen on the size distribution of nanostructured  $\beta$ -Ga<sub>2</sub>O<sub>3</sub> and SnO<sub>2</sub>.

**Key words:** Nanowires, nanobelts, Raman

## INTRODUCTION

The traditional vapor-liquid-solid (VLS) method for growing micron-sized whiskers involves the use of a “catalytic” seed particle that controls the diameter of the whiskers.<sup>1</sup> Nanowires can be prepared using the VLS method as the catalyst particle size is reduced to nanometer scale using processes such as laser ablation, sublimation, thin film, and the use of nanosized powders.<sup>2</sup> In contrast, we have described in an earlier publication that long nanowires of uniform diameter can be synthesized without the need for catalyst seed particles. Our process involves the dissolution of vapors into a thin film or a pool of low-melting metals at elevated temperatures. This dissolution leads to the formation of nanoscale compound nuclei that do not wet the molten metal surface. As a result, with increasing reaction time, crystal growth from the nuclei is one dimensional in nature and nanowires are formed. In our first set of experiments, silicon nanowires were synthesized from dissolution of Si into millimeter-scale

Ga droplets, which clearly revealed multiple nucleation and growth of nanowires.<sup>3</sup> In subsequent experiments, we showed that decomposition of SiH<sub>4</sub> over Ga films deposited on quartz substrates also yields Si nanowires.<sup>4</sup> This concept was also extended to the synthesis of  $\beta$ -Ga<sub>2</sub>O<sub>3</sub> nanowires from oxygen dissolution into Ga.<sup>5</sup> The morphology and size of the gallium oxide nanowires could be controlled using varying amounts of hydrogen along with oxygen. Following our studies, other nanostructures such as ZnO have been synthesized by direct heating of metallic Zn in an oxidizing environment.<sup>6</sup> Experiments involving high-temperature chemical vapor transport of metal oxide powders have also resulted in the growth of nanowires and nanobelts.<sup>7</sup> Here, we report a systematic study of low-melting metal oxide and sulfide nanostructures that form when respective metals are exposed to either oxygen or H<sub>2</sub>S at an elevated temperature.

## EXPERIMENTAL

The synthesis of the nanowires and nanobelts was performed using commercial powders of pure metals

of Ga, Sn, and In (Aldrich, St. Louis, MO). Quartz substrates with respective metal powders were placed in the center zone of a tubular quartz reactor (diameter  $\sim 1.5$  in.). The reactor was then heated to temperatures ranging from  $700^{\circ}\text{C}$  to  $1,200^{\circ}\text{C}$  at ambient pressure and under a continuous flow of argon (flow rate  $\sim 100$  sccm). At these elevated temperatures, the metal powders melt and form a thin film on the substrates. Once the temperature of the reactor stabilized, feed gases such as oxygen and hydrogen sulfide (flow rate  $\sim 400$  sccm) were intro-

duced into the reactor depending upon the desired material. The reaction time was typically an hour, after which the feed gas was turned off and the reactor was allowed to cool. Table I lists the experimental parameters used in the synthesis of various nanowires and nanobelts. Growth of nanostructures did not occur at temperatures higher or lower than the ranges listed in Table I. Similar experiments were also conducted in a vacuum chamber using 100 sccm gas flow containing (90–100 sccm) oxygen and (10–0 sccm) hydrogen.

**Table I. Experimental Conditions Used in This Study for the Growth of Different Nanostructures\***

Metal	Reaction	Product (Bandgap, eV)	Synthesis Temperature ( $^{\circ}\text{C}$ )	$\Delta G$ (kJ/mol)
Ga	$2\text{Ga(l)} + 1.5\text{O}_2 \Rightarrow \text{Ga}_2\text{O}_3$	$\beta\text{-Ga}_2\text{O}_3$ (4.8)	950–nanowires 1050–nanobelts	–689.7 –657.5
Ga	$2\text{Ga(l)} + 3\text{H}_2\text{S} \Rightarrow \text{Ga}_2\text{S}_3 + 3\text{H}_2$	$\alpha\text{-Ga}_2\text{S}_3$ (2.8)	650–800	–293.4 to –269.3
In	$2\text{In(l)} + 1.5\text{O}_2 \Rightarrow \text{In}_2\text{O}_3$	$\beta\text{-In}_2\text{O}_3$ (2.8)	1000–1200	–520.7 to –459.0
In	$2\text{In(l)} + 3\text{H}_2\text{S} \Rightarrow \text{In}_2\text{S}_3 + 3\text{H}_2$	$\text{In}_2\text{S}_3$ (2.82)	700–800	–137.1 to –123.8
Sn	$\text{Sn(l)} + \text{O}_2 \Rightarrow \text{SnO}_2$	$\text{SnO}_2$ (3.7)	900–1200	–339.9 to –276.6

\*Thermodynamic data from 2nd ed., *Thermochemical Properties of Inorganic Substances*. O. Knacke, O. Kubaschewski, and K. Hesselmann, (New York: Springer-Verlag), 1991.

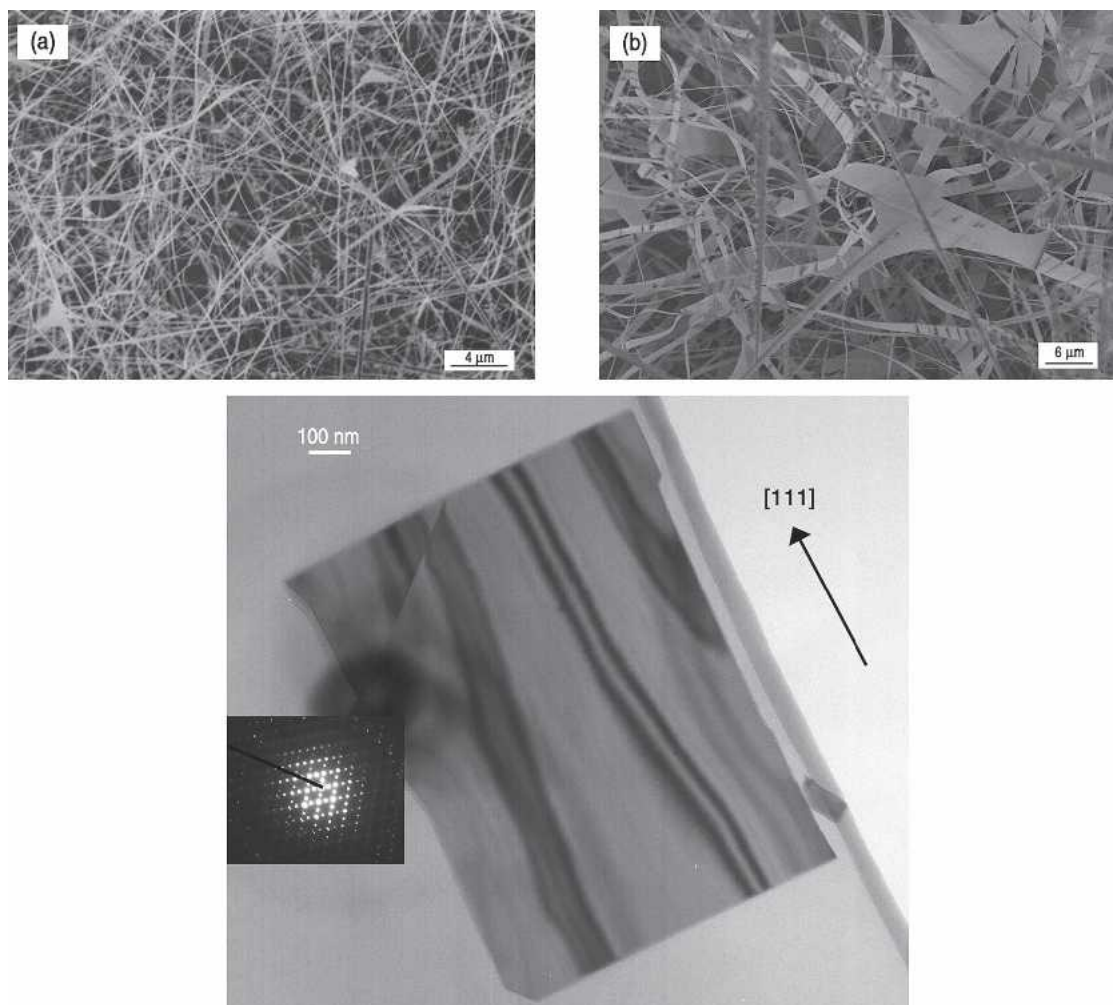


Fig. 1. SEM images of  $\beta\text{-Ga}_2\text{O}_3$  (a) nanowires and (b) nanobelts synthesized at  $950^{\circ}\text{C}$  and  $1,050^{\circ}\text{C}$ , respectively. (c) HRTEM image of a single  $\beta\text{-Ga}_2\text{O}_3$  nanobelt along the [111] growth direction. Inset is a SAD pattern revealing the monoclinic structure.

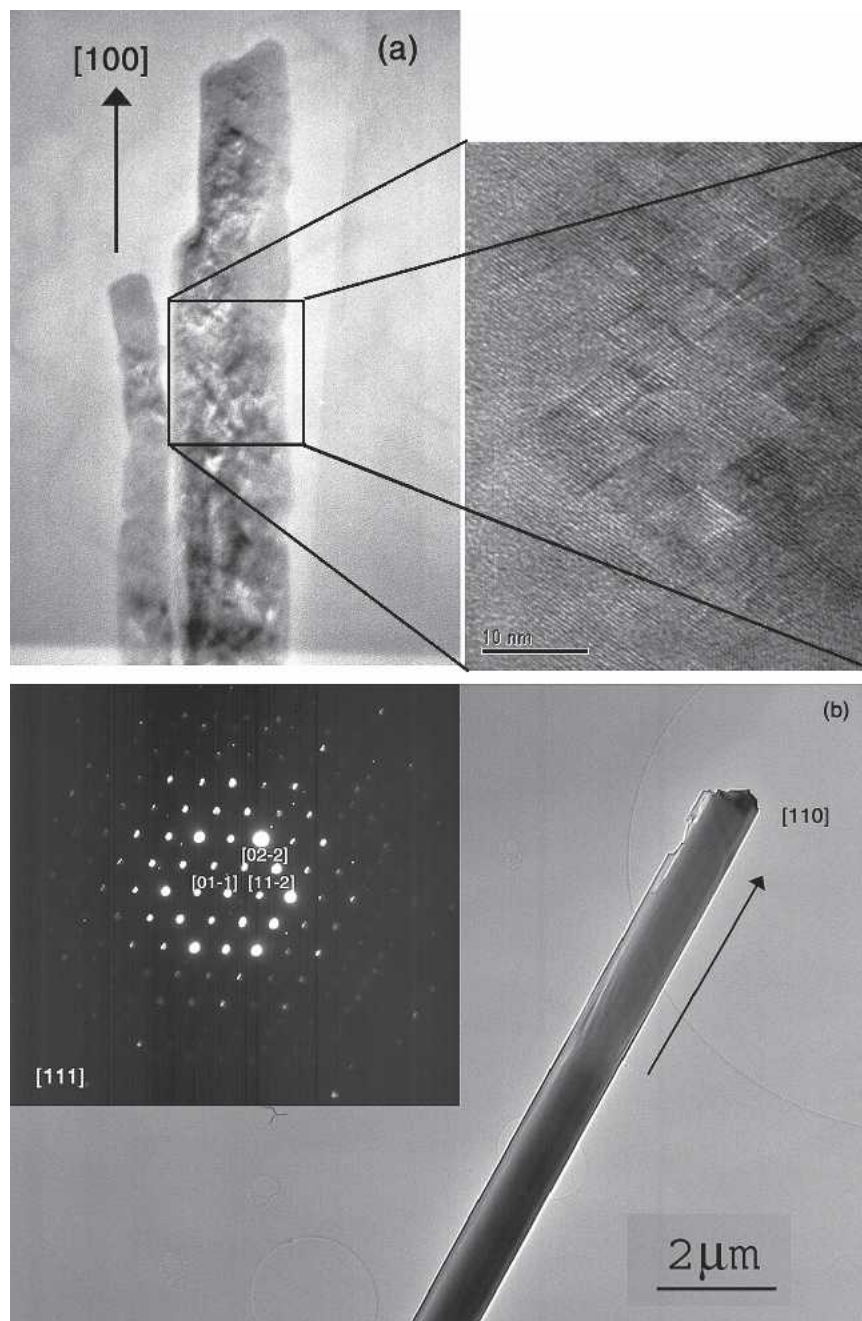


Fig. 2. (a) HRTEM image of a  $\alpha$ - $\text{Ga}_2\text{S}_3$  nanowire showing twinning shown in detail in the inset figure. (b) HRTEM image of a  $\beta$ - $\text{In}_2\text{S}_3$  nanowire exhibiting tetragonal crystal structure (inset figure shows the SAD pattern).

The morphology of the as-prepared nanomaterials was analyzed via scanning electron microscopy (model Hitachi S-4700) (Hitachi, Pleasanton, CA), high-resolution transmission electron microscopy [HRTEM model JEOL 3,010 (Japan Electron Optics Ltd., Tokyo)], and electron diffraction. The analysis of the selected area diffraction (SAD) patterns was performed with the help of simulations using a software package (Desktop Microscopist from the NCEM-LBL) (Lawrence Berkeley National Labs, Berkeley, CA). The nanowires and nanobelts were dispersed in acetone using ultrasonication for  $\sim 30$

sec or until a uniform dispersion was obtained. A few drops of the dispersion were then used on a 200-mesh holey carbon transmission electron microscopy (TEM) Cu grid [electron microscopy sciences (EMS)]. Optical characterization was performed on the as-synthesized samples using room-temperature micro-Raman spectroscopy (model Renishaw 1000) with an excitation wavelength of 785 nm. Photoluminescence was measured using a Renishaw inVia spectrometer (Renishaw Inc., Hoffman Estates, IL) (330–1,000 nm range) with the 325-nm excitation from a He-Cd laser.

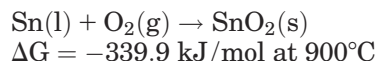
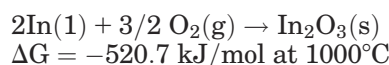
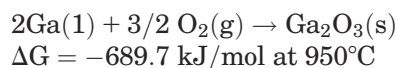
## RESULTS AND DISCUSSION

The thermal oxidation of gallium melts using oxygen at atmospheric pressure resulted in the growth of  $\beta$ - $\text{Ga}_2\text{O}_3$  nanostructures whose morphologies varied from nanowires to nanobelts, as shown in Fig. 1. The quartz substrates were covered evenly with nanowires having diameters between 10 nm and 100 nm. The monoclinic crystal structure of the samples depicted in Fig. 1 was confirmed through electron diffraction and micro-Raman spectroscopy. When the reaction temperature was increased from 950°C to 1,050°C, a significant amount of  $\beta$ - $\text{Ga}_2\text{O}_3$  nanobelts were formed relative to the nanowires present on the substrate (Fig. 1b). The widths of the nanobelts ranged between 100 nm and  $\sim 1 \mu\text{m}$ , with an average thickness of  $\sim 50$  nm. Electron diffraction studies showed the growth direction of the nanobelts to be in the [111] direction (Fig. 1c). Such a temperature-induced abrupt change in the morphology of nanostructures has been reported previously. Recently, Sun et al.<sup>8</sup> synthesized  $\text{SnO}_2$  nanowires and nanobelts by carbothermal reduction of  $\text{SnO}_2$  powder mixed with graphite at ambient pressure. Consistent with our results in Fig. 1, they found  $\text{SnO}_2$  nanowires in the relatively low-temperature region of their reactor ( $\sim 600$ – $750^\circ\text{C}$ ), while nanobelts were found in regions where the temperature was  $\sim 950$ – $1,000^\circ\text{C}$ . Based on four different morphologies that were observed in their reactor, they attribute the change in morphology to preferential growth along directions normal to the growth direction of the nanowire.<sup>8</sup> In order to understand similar changes in the morphology of gallium oxide nanostructures, we note that the vapor pressure of Ga does not increase linearly throughout the temperature range between 30°C and 1,200°C, but increases exponentially.<sup>9</sup> The predominant growth of  $\beta$ - $\text{Ga}_2\text{O}_3$  nanobelts occurred only when the synthesis temperature exceeded the critical temperature of 1,000°C. At 950°C, Ga has a vapor pressure of  $1.4 \times 10^{-3}$  torr, and at 1,050°C, it has a vapor pressure of  $1.0 \times 10^{-2}$  torr.<sup>10</sup> Based on this, it is reasonable to expect that the nanobelt growth occurs due to direct growth from the vapor phase onto the sides of the growing nanowires. This type of regrowth could be responsible for the change in wirelike to beltlike morphology due to enhanced growth in certain directions. In our studies, a similar temperature-induced change in morphology was also observed in oxidation experiments involving tin. However, we did not observe a similar trend in experiments involving indium and a further study is needed.

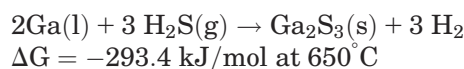
Figure 2a and b show HRTEM images of  $\alpha$ - $\text{Ga}_2\text{S}_3$  and  $\beta$ - $\text{In}_2\text{S}_3$  nanowires, respectively, and were obtained when respective metals were exposed to  $\text{H}_2\text{S}$  at elevated temperatures at ambient pressure (see Table I). To our knowledge, these nanostructures have not been previously reported, or examined in detail, in the literature, with the exception of one report on indium sulfide nanorods using decomposition

of a metalorganic precursor,  $\text{Et}_2\text{In}(\text{S}_2\text{CNMe}^n\text{Bu})$ , which was reported by Afzaal et al.<sup>11</sup> In our study, the monoclinic  $\alpha$ - $\text{Ga}_2\text{S}_3$  nanowires exhibited [100] growth direction and appear to be twinned, as seen in the inset image in Fig. 2a. Furthermore, their diameters ranged between 15 nm and 200 nm and their lengths measured a few micrometers. Similarly, the growth direction for the tetragonal  $\beta$ - $\text{In}_2\text{S}_3$  nanowires was found to be along the [110] direction (Fig. 2b). Consistent with electron microscopy results, micro-Raman spectra for each nanowire listed in Table I confirmed the crystalline nature for each of these nanostructures (Fig. 3). It should be mentioned that the corresponding nitride nanowires and nanobelts were also prepared in the presence of  $\text{NH}_3$  and will be discussed elsewhere.

The direct reactions could be understood through straightforward thermodynamic analysis. In the case of reactions involving molten metals and oxygen, molecular oxygen is sufficiently reactive with either Ga, In, or Sn forming nanometer-sized metal-oxide nuclei. As an example, the Gibbs free energy ( $\Delta G$ ) values<sup>12</sup> for the oxide nanostructures are listed below:



These  $\Delta G$  values listed above (also listed in Table I) suggest that the metal-oxide reactions can proceed under the experimental conditions used in this study. Similarly, the chemical reaction for the formation of gallium sulfide nanowires is as follows:



Based on the value of  $\Delta G$ , the above reaction is favorable for the growth of sulfide nanowires by

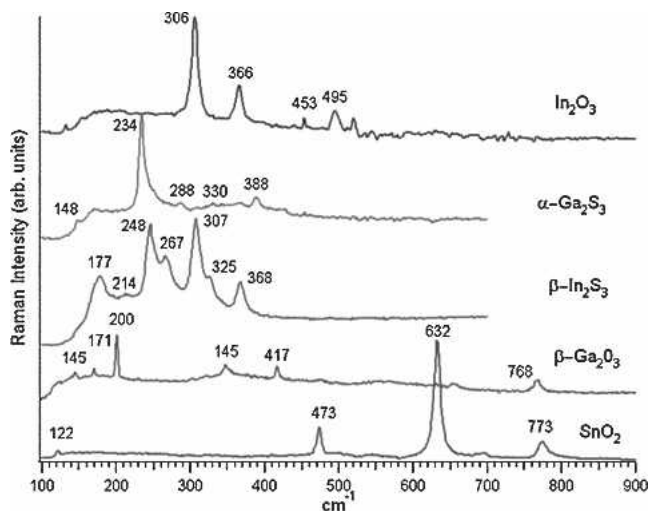


Fig. 3. Micro-Raman spectra from semiconducting nanowires.

direct reaction of  $H_2S$  at the metal surface. The possible route for direct reaction must involve catalyzed decomposition on the molten Ga surface to provide sulfur dissolution into the Ga melt. The decomposition of  $H_2S$  on metal surfaces is known to occur,<sup>13</sup> but no detailed studies have been reported with respect to gallium. The dissolution of sulfur into Ga melts would lead to the formation of nanometer scale nuclei, which enable nanowire growth, as in the case of the oxide nanowires. The presence of hydrogen resulting from the decomposition of  $H_2S$  is expected to play a similar role as in the oxide nanostructures and is discussed below. A similar scheme is expected for indium sulfide nano-

structures with direct reaction of indium melt with  $H_2S$ .

The formation of nanoscale oxide or sulfide nuclei on the molten metal surfaces is not a sufficient criterion for the growth of nanoscale nuclei into nanowires. It is also important that the nanometer-sized nuclei do not wet the molten metal surfaces. No experimental data exist on the interfacial energy values for these inorganic solid-liquid systems. So, using Neumann's equation of state,<sup>14</sup> the contact angles between the liquid metal and solid compound phases were estimated to be around  $180^\circ$ , confirming that the solid and liquid phases do not wet each other in the absence of any other chemisorbed

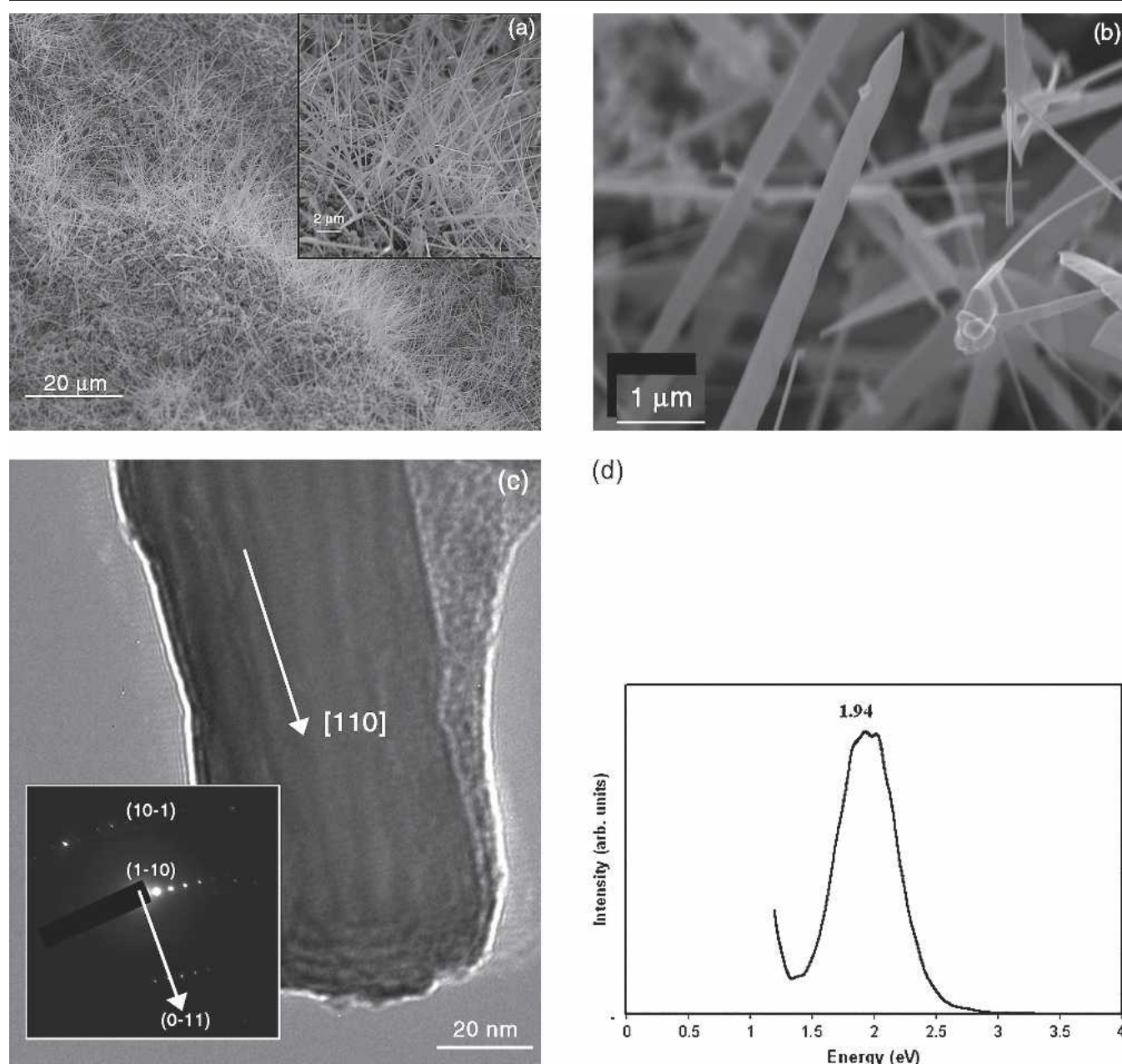


Fig. 4. (a) SEM figure of  $SnO_2$  nanowires prepared at  $900^\circ C$ . The inset is a blown up image of the nanowires. (b) SEM image of  $SnO_2$  nanobelts prepared at  $1,200^\circ C$ . (c) HRTEM image of a single  $SnO_2$  nanowire and the corresponding diffraction pattern. (d) Photoluminescence spectrum of  $SnO_2$  nanowires.

species on either phase.<sup>5</sup> With increasing reaction time, these nuclei evolve into one-dimensional nanostructures due to their nonwetting characteristics. In the presence of hydrogen, the low-melting metals maintain high surface tension necessary for the growth of nanowires from the nanoscale nuclei through basal attachment.

The effect of hydrogen is illustrated using tin oxide nanowire growth at low pressures as an example. Metallic tin powder dispersed on a quartz substrate was heated to 900°C in a growth chamber maintained at 0.4 torr dynamic vacuum. Thick polycrystalline SnO<sub>2</sub> crust with few nanowires resulted when 100 sccm of oxygen was used as the feed gas. However, a dramatic increase in the nanowire yield was observed as hydrogen was mixed into the feed gas. A mixture of 10/90 sccm of hydrogen/oxygen resulted in the optimal growth of tin oxide nanowires, and a SEM image is shown in Fig. 4a. Multiple nucleation and growth of nanowires is evident. As the substrate temperature was increased from 900°C to 1,200°C in the presence of hydrogen (10 sccm) and oxygen (90 sccm), the thickness of the resulting nanowires increased and was accompanied with a change in morphology from nanowires to nanobelts (width of ~300 nm and thickness ~70 nm), as shown in Fig. 4b. From the TEM diffraction patterns (inset figure in 4c), the growth direction of the resulting nanowires was determined to be [110]. The growth of wirelike morphology results due to multiple nucleation and basal growth from molten metal pools, while the beltlike morphology seems to result with chemical vapor deposition of tin oxide from the vapor phase onto the growing nanowires. Further reduction in synthesis temperatures is only possible when atomic hydrogen is supplied instead of molecular hydrogen, i.e., either through hot-filament activation or plasma activation, as described in our earlier work on gallium oxide nanowires using plasma-activated hydrogen/oxygen gas phase and chamber temperatures ~400–500°C.<sup>5</sup> The PL spectrum of tin oxide nanowires grown at 0.4-torr chamber pressure exhibits yellow luminescence (Fig. 4d), which can be attributed to oxygen deficiency in the nanowires. The origin of the oxygen deficiency could

be due to thermal aging of the nanowires under the conditions used in our experiments.

## SUMMARY

In conclusion, we have presented a simple and scaleable thermal synthesis technique for low-melting metal oxide and sulfide nanowires. Our technique is based on the dissolution of oxygen or sulfur gases into low-melting metal pools, which result in one-dimensional structures of the respective compounds. It is clear from the studies presented here that our synthesis method can be easily extended to other low-melting metallic systems, as well as a variety of compounds such as phosphides, nitrides, and arsenides depending upon the choice of feed gas.

## REFERENCES

1. R.S. Wagner and W.C. Ellis, *Appl. Phys. Lett.* 4, 89 (1964).
2. (a) A.M. Morales and C.M. Leiber, *Science*, 279, 208 (1998). (b) J. Westwater, D.P. Gosain, S. Tomiya, S. Usui, and H. Ruda, *J. Vac. Sci. Technol. B*, 15, 554 (1997). (c) S. Sharma, H. Li, H. Chandrasekaran, R.C. Mani, and M.K. Sunkara, in *The Encyclopedia of Nanoscience and Nanotechnology*, ed. H.S. Nalwa (Los Angeles, CA: American Scientific Publishers, 2004), vol. 10, pp. 327–346.
3. M.K. Sunkara, S. Sharma, R. Miranda, G. Lian, and E.C. Dickey, *Appl. Phys. Lett.* 79, 1546 (2001).
4. S. Sharma and M.K. Sunkara, *Nanotechnology* 15, 130 (2004).
5. S. Sharma and M.K. Sunkara, *J. Am. Chem. Soc.* 124, 12288 (2002).
6. H.Y. Dang, J. Wang, and S.S. Fan, *Nanotechnology* 14, 738 (2003).
7. Z.W. Pan, Z.R. Dai, and Z.L. Wang, *Science* 291, 1947 (2001).
8. S.H. Sun, G.W. Meng, M.G. Zhang, X.H. An, G.S. Wu, and L.D. Zhang, *J. Phys. D: Appl. Phys.* 37, 409 (2004).
9. I.A. Sheka, I.S. Chaus, and T.T. Mityureva, *The Chemistry of Gallium* (New York: Elsevier Pub. Co., 1966).
10. in *CRC Handbook of Chemistry and Physics*, D.R. Lide, ed. (Boca Raton, FL: CRC Press, 2003-04), pp. 4–134.
11. M. Afzaal, M.A. Malik, and P. O'Brien, *Chem. Commun.* 3, 334 (2004).
12. *Thermodynamic Data from Thermochemical Properties of Inorganic Substances*, 2nd ed., ed. O. Knacke, O. Kubaschewski, and K. Hesselmann (New York: Springer-Verlag, 1991), pp. 717–1893.
13. J. Zaman and A. Chakma, *Fuel Proc. Technol.* 41, 159 (1995).
14. D. Li and A.W. Neumann, *Adv. Coll. Interfacial Sci.* 39, 299 (1992).